Earth and Planetary Science Letters 434 (2016) 220–230

Contents lists available at ScienceDirect

Earth and Planetary Science Letters

www.elsevier.com/locate/epsl

New magnetochronology of Late Miocene mammal fauna, NE Tibetan Plateau, China: Mammal migration and paleoenvironments

Hong Ao [a,*], Peng Zhang [a], Mark J. Dekkers [b], Andrew P. Roberts [c], Zhisheng An [a], Yongxiang Li [d], Fengyan Lu [a], Shan Lin [a,e], Xingwen Li [a,e]

[a] State Key Laboratory of Loess and Quaternary Geology, Institute of Earth Environment, Chinese Academy of Sciences, Xi'an 710075, China
[b] Paleomagnetic Laboratory 'Fort Hoofddijk', Department of Earth Sciences, Faculty of Geosciences, Utrecht University, Budapestlaan 17, 3584 CD Utrecht, The Netherlands
[c] Research School of Earth Sciences, The Australian National University, Canberra 2601, Australia
[d] State Key Laboratory of Continental Dynamics, Department of Geology, Northwest University, Xi'an 710069, China
[e] University of Chinese Academy of Sciences, Beijing 100049, China

ARTICLE INFO

Article history:
Received 27 July 2015
Received in revised form 9 November 2015
Accepted 14 November 2015
Available online 10 December 2015
Editor: A. Yin

Keywords:
magnetostratigraphy
Stegodon
mammal migration
paleoenvironment
Tibetan Plateau
Late Miocene

ABSTRACT

Lanzhou Basin lies on the northeastern margin of the Tibetan Plateau in western China and is a rich source of Oligocene–Miocene mammalian fossils. Obtaining precise age determinations for these fossils is important to address key questions concerning mammalian and environmental evolution in Asia associated with stepwise Tibetan Plateau uplift. Here we report a new magnetostratigraphic record for the Xingjiawan fluvio-lacustrine section from the northwestern margin of Lanzhou Basin that can be correlated to the geomagnetic polarity timescale with two options. The Late Miocene Xingjiawan Fauna is located either at the boundary between reversed polarity chron C4r.1r and normal polarity chron C4n.2n or at the boundary between subchrons C5r.1r and C5n.2n, with an estimated age of at least ~8 Ma or perhaps as early as ~11 Ma. Both age estimations imply that the fossil *Stegodon* in the Lanzhou Basin is the oldest known record of *Stegodon* worldwide; it predates the formerly oldest *Stegodon* find from Africa by at least one million years and perhaps by as many as four million years. This provides new evidence for an Asian origin of *Stegodon*. Together with other faunal components, a mixed woodland/grassland setting existed in the Lanzhou Basin during the Late Miocene, in contrast to its modern arid environment.

1. Introduction

Widely occurring Cenozoic continental strata in western China contain diverse terrestrial faunal assemblages (Wang et al., 2013). However, at present the ages of most fossiliferous successions are poorly constrained by their biochronology. Lack of precise numerical ages makes robust calibration of the chronology of these faunas problematical, and complicates in-depth investigation of mammalian evolution and migration patterns in this key region. Furthermore, linkage to regional and global environmental changes is complicated by the absence of a reliable age model. The long terrestrial sedimentary sections in western China are generally devoid of suitable material for radiometric dating. Therefore, integrated bio-magnetostratigraphy has become the method of choice to resolve dating issues on timescales of 10^5 yr within a biogeographic province (e.g., Flynn et al., 1997).

Lanzhou Basin (Fig. 1) is located on the northeastern margin of the Tibetan Plateau, northwest China. It hosts one of the most complete Oligocene–Miocene terrestrial mammal assemblages in China. In order to numerically date these faunas, Opdyke et al. (1998) conducted a first magnetostratigraphic study of the Duitinggou section (36°13′N, 103°37′E) in southeastern Lanzhou Basin (Fig. 1). However, their magnetostratigraphy has comparatively low-resolution with large stratigraphic intervals between samples (1–5 m) that precluded unequivocal correlation to the geomagnetic polarity timescale (GPTS). As a result, distinctly different age correlations have been suggested (Opdyke et al., 1998; Flynn et al., 1999; Qiu et al., 2001, 2013). Three other magnetostratigraphic studies were conducted on the Yongdeng (36°22′N, 103°30′E) (Yue et al., 2001), Nanshan (36°01′N, 103°51′E) (Sun et al., 2011), and Fenghuangshan (36°12′N, 103°33′E) (Zhang et al., 2014) sections to generate age models for paleoenvironmental interpretations. However, these studies were not integrated with fossil mammal records. Therefore, the ages of these faunas have long been controversial.

* Corresponding author.
E-mail address: aohong@ieecas.cn (H. Ao).

http://dx.doi.org/10.1016/j.epsl.2015.11.019
0012-821X/

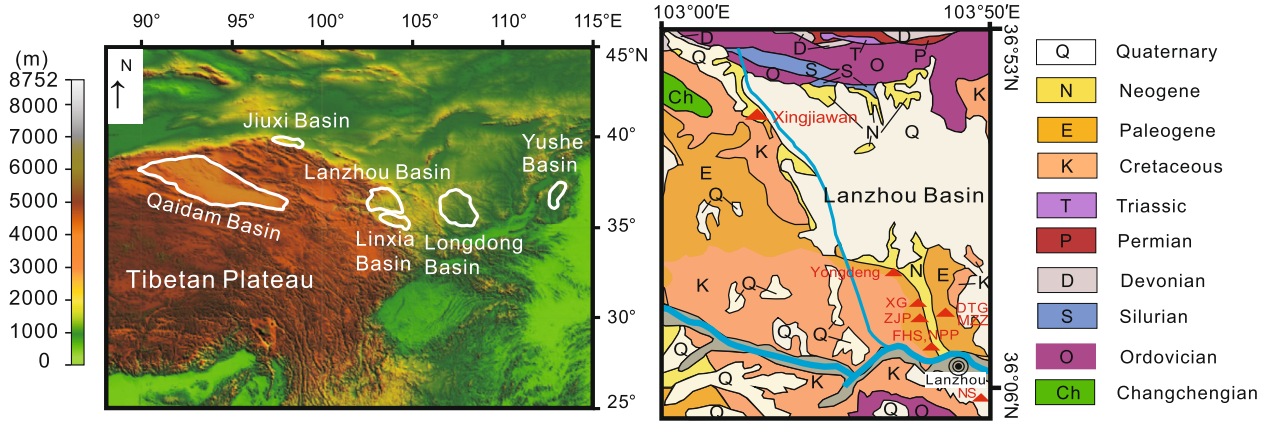

Fig. 1. Locations of Lanzhou Basin, faunal or section sites (red triangles) and other basins mentioned in the text. XG, Xiagou; ZJP, Zhangjiaping; DTG, Duitinggou; MZZ, Miaozuizi; NPP, Nanpoping; FHS, Fenghuangshan; and NS, Nanshan.

The Xingjiawan locality (36°46′N, 103°13′E) is a Late Miocene faunal site (Zhang, 1993) located on the northwestern margin of Lanzhou Basin (Fig. 1), which has not been sampled for magnetostratigraphy before. Here, we provide age constraints on this fauna with a detailed magnetostratigraphic study of a well-exposed succession of fluvio-lacustrine sediments. Combined magnetochronological controls and faunal composition analysis offer an important window into mammalian and paleoenvironmental evolution on the northeastern margin of the Tibetan Plateau.

2. General setting

Lanzhou Basin has a semi-arid continental climate and is situated in the transitional belt between humid southeast China, which is under the influence of the East Asian monsoon, and arid areas in the northwest. The modern natural vegetation is sparse and shifts gradually from semi-arid grassland to arid grassland from the southeast to the northwest of the basin (Huang, 1986; Jiang et al., 2011). The vegetation is mainly composed of herbs and dwarf shrubs, with a few patches of forest on the surrounding mountains and along the edges of foothills or tablelands (Huang, 1986; Jiang et al., 2011). The basin contains fluvio-lacustrine deposits, more than 1000 m thick, which range in age from the Paleocene to Miocene. From older to younger, the Xiliugou, Yehucheng and Xianshuihe Formations are distinguished based on sediment lithology (Zhai and Cai, 1984). The lowermost Xiliugou Formation consists of red massive sandstones and gravelly sandstones. The overlying Yehucheng Formation consists of distinctive dark red gypsiferous mudstone, siltstone, and sandstone units. The uppermost formation, the Xianshuihe Formation of Oligocene–Miocene age, mainly consists of red mudstones that are intercalated with sandstone or conglomerate packages. It is a rich source of mammalian fossils, with more than 90 localities yielding large and/or small mammals, such as the well-known faunas of Xingjiawan, Duitinggou, Zhangjiaping, Miaozuizi, Nanpoping and Xiagou (Zhang, 1993; Qiu et al., 2001; Xie, 2004).

At the Xingjiawan section, the upper part of the Xianshuihe Formation is exposed with a bedding attitude of strike 330° and dip 6° to the NE. The sampled succession has a stratigraphic thickness of 217.4 m: it mainly consists of red mudstone, intercalated with siltstone, sandstone, conglomeratic sandstone, and conglomerate layers. The frequent occurrence of coarse-grained lithologies (conglomeratic sandstone and conglomerate) is inferred to be due to the combined effects of local tectonic activity and high-energy floods/riverine input.

The Xingjiawan faunal layer occurs in mudstone at the 190–195-m depth interval (where 0 m is at the top of the section). An earlier excavation yielded more than 20 fossils, including 6 identified species: *Stegodon* sp., *Cervidae* indet., *Chilotherium haberei*, *Hipparion* sp., *Chleuastochoerus stehlini* and *Hyaena variabilis* (Zhang, 1993). All 6 species are common components of the Late Miocene *Hipparion* Fauna in North China (Zhang, 1993), but a precise age for the faunal layer cannot be determined on the basis of the fossils alone. In addition, more than 1000 kg of fossils have been excavated by local farmers and have been sold as medicinal "dragon bones". Unfortunately, the respective mammal species are not known. We also found mammalian bone fragments during paleomagnetic field sampling.

3. Sampling and methods

In order to obtain samples that were as fresh as possible, weathered surfaces were removed from the outcrop (at least the surface-most 20 cm). From the entire Xingjiawan section, 486 block samples were taken from siltstone, sandstone and conglomeratic sandstone layers (conglomeratic layers were not sampled), and were oriented using a magnetic compass in the field. From each block sample, two cubic (2 cm × 2 cm × 2 cm) specimens were cut in the laboratory for thermal demagnetization experiments. Leftover sediment was used to determine the magnetic mineralogy from temperature-dependent susceptibility (κ–T) and isothermal remanent magnetization (IRM) acquisition measurements.

About 300 mg of powdered material was used to measure κ–T curves with a Kappabridge magnetic susceptibility meter (model KLY-3) equipped with a CS-3 high-temperature furnace (AGICO Ltd., Brno, Czech Republic) in an argon atmosphere (with a flow rate of 100 mL/min) from room temperature to 700 °C and back to room temperature. A κ run with an empty furnace tube was measured to determine the temperature-dependent background before measuring the sediment samples. The susceptibility of each sediment sample was obtained by subtracting the measured background κ (furnace tube correction) using the CUREVAL 5.0 program (AGICO, Brno, Czech Republic). These experiments were carried out at the Institute of Geology and Geophysics, Chinese Academy of Sciences (IGGCAS), Beijing, China.

Six non-magnetic cubic boxes (2 cm × 2 cm × 2 cm) filled with powdered sediment were magnetized with an impulse magnetizer (model IM-10-30) and the IRMs were measured with an AGICO JR-6A dual speed spinner magnetometer in a magnetically shielded laboratory. IRM acquisition curves were measured at 30 field steps up to a maximum field of 2 T. These experiments were carried out at the Institute of Earth Environment, Chinese Academy of Sciences (IEECAS), Xi'an, China.

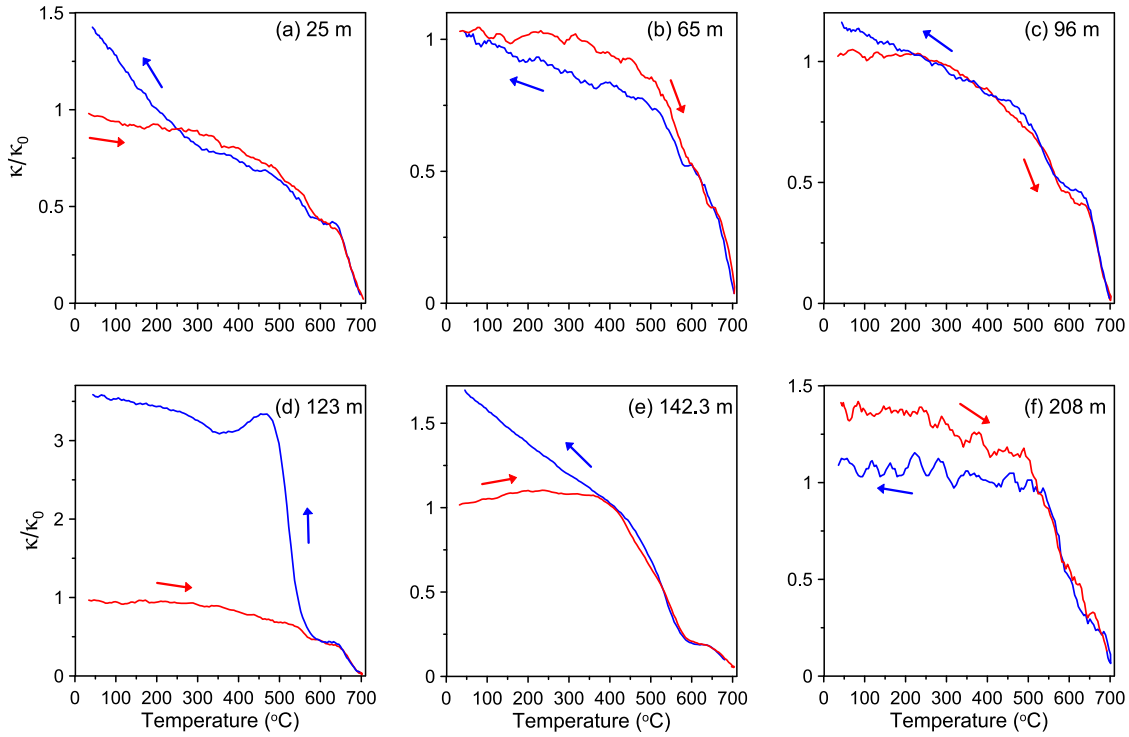

Fig. 2. Temperature dependence of magnetic susceptibility (κ–T) for typical samples from the Xingjiawan section. κ_0 is the starting value of the magnetic susceptibility at room temperature. Red (blue) lines represent heating (cooling) curves. (For interpretation of the references to color in this figure legend, the reader is referred to the web version of this article.)

Progressive thermal demagnetization of the natural remanent magnetization (NRM) was conducted using a TD-48 thermal demagnetizer at IEECAS or at the Institute of Tibetan Plateau Research, Chinese Academy of Sciences (ITPRCAS), Beijing, China. All samples were stepwise heated in 18 steps at 10–50 °C increments to a maximum temperature of 680 °C. After each demagnetization step, the remaining NRM was measured using a 2-G Enterprises superconducting quantum interference device magnetometer housed in a magnetically shielded laboratory. The NRM intensity was usually of the order of 10^{-4} to 10^{-2} A/m, while the instrumental background (or noise) magnetization level in the magnetometer is generally of the order of 10^{-7} to 10^{-6} A/m (for a sample volume of 8 cm^3). Results were evaluated using orthogonal vector demagnetization diagrams (Zijderveld, 1967); the characteristic remanent magnetization (ChRM) was determined by principal component analysis (PCA) for each sample (Kirschvink, 1980). PCA was done with the PaleoMag software of Jones (2002); the least-squares linear fits were anchored to the origin of the diagrams. Not all collected samples were subjected to paleomagnetic measurements. Samples were first measured at 1-m stratigraphic intervals. If polarity divisions were not clearly suggested in certain intervals, additional stratigraphic levels were measured at 30-cm and even 10-cm sampling resolution until a detailed and unambiguous polarity sequence was established for the Xingjiawan section. In total, samples from 378 stratigraphic levels were subjected to paleomagnetic measurements for this purpose.

4. Results

4.1. Magnetic mineralogy

The low-field magnetic susceptibility of hematite is about two orders of magnitude lower than that of magnetite (Dunlop and Özdemir, 1997). Therefore, the presence of hematite is usually masked magnetically by the much stronger contribution of magnetite, and its expression on κ–T curves is generally subdued when both magnetite and hematite are present. However, κ–T heating curves for typical samples from the Xingjiawan section are characterized by a distinct drop in κ between 580 and 680 °C (Fig. 2), which indicates the presence of abundant hematite, in agreement with the red color of the mudstone beds. The κ–T heating curves also undergo a marked κ decrease at 500–600 °C, which indicates the ubiquitous presence of small amounts of magnetite in the studied sediments. Some cooling curves increase sharply below ca. 300–400 °C (Fig. 2a, e). This is possibly due to formation of fine-grained magnetite at high temperature (possibly >500 °C) during thermal treatment, which becomes superparamagnetic below ~300 °C and is paramagnetic above that temperature (Jiang et al., 2015).

Consistent with the dominant presence of high-coercivity hematite in the Xingjiawan fluvio-lacustrine sediments, the IRM gradually increases with field strength; it is unsaturated in fields up to 2 T, the maximum field strength available for the equipment used to impart the IRM (Fig. 3). Cumulative log-Gaussian decomposition analysis of IRM acquisition curves (Kruiver et al., 2001) indicates two components: a variable low-coercivity component (magnetite) and a variable high-coercivity component (hematite) (Fig. 3 and Table S1). The variability of these components reflects variable grain sizes of these minerals in different samples and lithologies. High-coercivity hematite contributes dominantly (> ~60%) to the acquired IRM in 4 of 6 measured samples, while in the other 2 samples the contribution of low-coercivity magnetite is more significant (Table S1). On a mass-specific basis, however, magnetite has an IRM that is about two orders of magnitude stronger than hematite (Dunlop and Özdemir, 1997), so large hematite concentrations are necessary for hematite to contribute substantially to the remanence when magnetite is also present. Therefore, IRM acquisition curves and cumulative log-Gaussian decomposition analysis point to the dominance of hematite and to relatively minor magnetite contents in the Xingjiawan fluvio-lacustrine sediments.

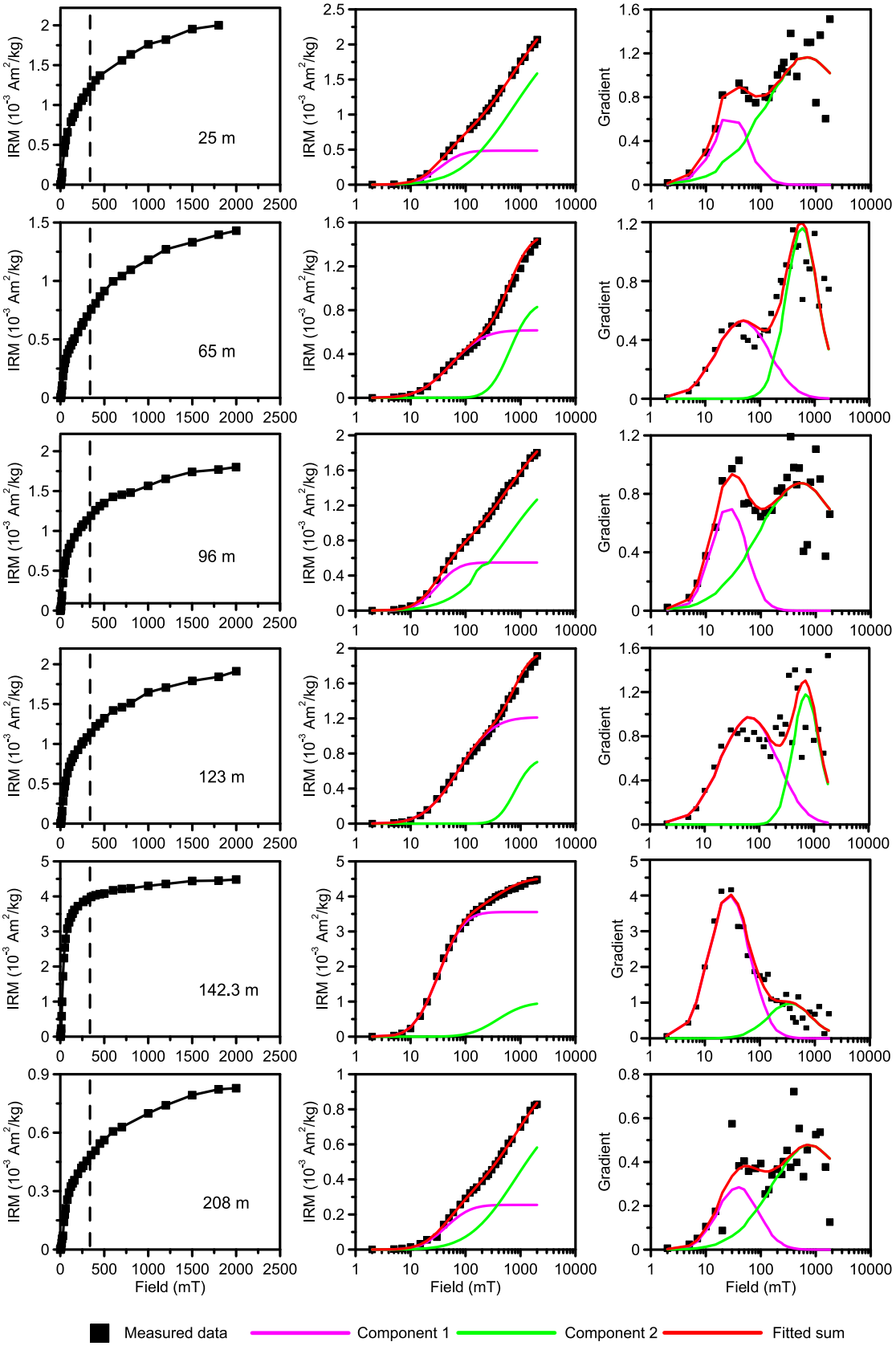

Fig. 3. Isothermal remanent magnetization (IRM) acquisition curves plotted versus linear and logarithmic field axes, and gradient acquisition plots (according to the terminology of Kruiver et al., 2001) for typical samples (the same samples as in Fig. 2) from the Xingjiawan section. The dashed vertical lines at 300 mT are shown to aid distinction between low- and high-coercivity portions of the IRM acquisition curves.

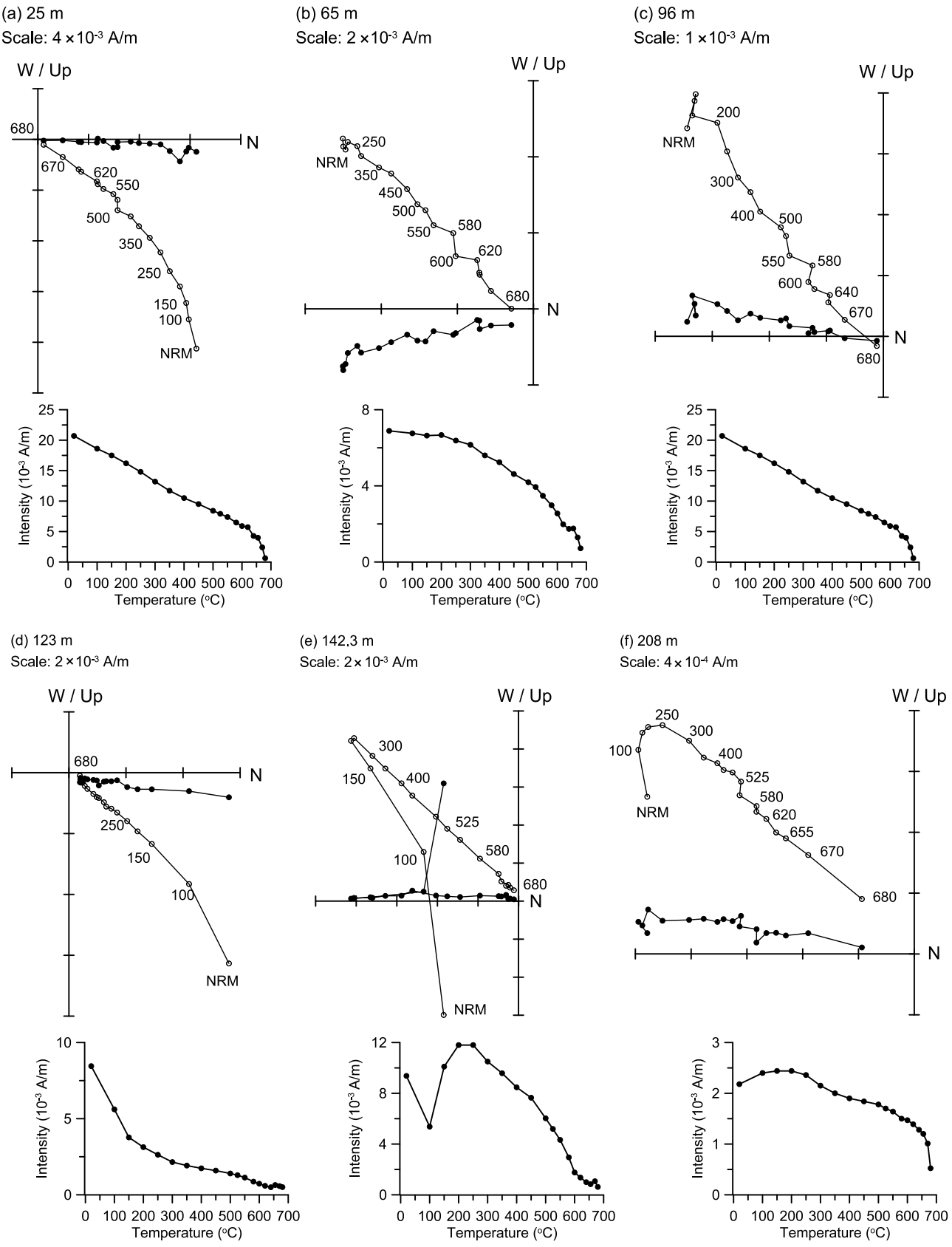

Fig. 4. Evolution of the direction and intensity of the NRM during stepwise thermal demagnetization for selected samples with stable paleomagnetic data from the Xingjiawan section (the same samples as in Figs. 2 and 3). Solid (open) circles represent projections onto the horizontal (vertical) plane (Zijderveld, 1967). Numbers refer to demagnetization temperatures in °C. NRM values on the demagnetization diagrams refer to the NRM at room temperature.

4.2. Paleomagnetism

Our detailed paleomagnetic analysis involved removal of secondary magnetizations by thermal demagnetization to 250 °C, and isolation of the ChRM during stepwise heating to 680 °C (Fig. 4). In general, the ChRM is characterized by a relatively straightforward unidirectional trajectory toward the origin of orthogonal vector demagnetization plots from 200–300 °C to 680 °C. In most samples, a gradual remanence decay occurs from 250 °C to 680 °C, with a minor additional drop near the Curie temperature of magnetite (~580 °C) (Fig. 4). This demagnetization behavior is consistent with hematite being the major ChRM carrier as suggested by the aforementioned rock magnetic results (Figs. 2 and 3), although magnetite may also be an important ChRM carrier in some samples. The same ChRM directions are observed for the 250–580 °C and 600–680 °C parts of the unblocking spectra. Therefore, the ChRM is due to hematite and magnetite, which both recorded the same paleomagnetic field when their remanences became locked-in within the sediments. Our observations are fully compatible with acquisition of a detrital remanent magnetization (Charreau et al., 2005).

Of the 378 levels demagnetized, 250 yielded stable ChRM components (cf. Fig. 5 and Table S2) based on strict selection criteria. Data from at least 4 (but typically 8–15) consecutive demagnetization steps were used to determine the ChRM direction starting at least at 250 °C, with a maximum angular deviation (MAD) $<15°$ for the respective line fits. Of the 250 ChRM directions, 24 are not considered further because they record inclinations $<5°$, or declinations that trend roughly north (or south) but with upward (or downward) inclinations inconsistent with the expected geomagnetic field direction (cf. Table S2 and Figs. S1 and S2). The other 128 demagnetized levels did not yield reliable ChRM directions and were excluded because they have unstable demagnetization trajectories at higher temperatures (e.g., Fig. S1a). For Cenozoic red beds from western China, it is common to have relatively high proportions of excluded samples, even in fine-grained lithologies (Dupont-Nivet et al., 2007).

Virtual geomagnetic pole (VGP) latitudes calculated from all the 226 (60%) reliable ChRM directions are used to establish the magnetostratigraphic zonation, which allows identification of 9 normal and 8 reversed polarity zones (Fig. 5). Each polarity zone is defined based on at least two consecutive VGP latitudes of identical polarity. The jackknife technique (Tauxe and Gallet, 1991) is useful to test the robustness of a magnetic polarity zonation. The obtained jackknife parameter (J) has a value of -0.0825 (Fig. 6), which falls within the range of 0 to -0.5 that was recommended for a robust magnetostratigraphic data set by Tauxe and Gallet (1991). This supports our interpretation that our magnetostratigraphy has recovered close to the true number of polarity intervals within the Xingjiawan section. The 226 reliable ChRM directions have an antipodal distribution with 134 normal and 92 reversed polarity directions (Fig. 7), although the reversals test (Tauxe, 1998) is negative at the 95% confidence level due to an offset between the mean normal and reversed polarity inclinations. Similar offsets have been observed for paleomagnetic data from the neighboring Xining Basin (west of Lanzhou Basin) and the Tianshan range (further northwest of Lanzhou Basin), which were interpreted to result from incomplete removal of the normal polarity overprint in some samples (Charreau et al., 2005; Dupont-Nivet et al., 2007; Xiao et al., 2012). However, as indicated by VGP latitudes (Fig. 5d), this offset does not affect polarity assignment. Determination of normal and reversed polarities is reliable, but caution should be exercised in using these paleomagnetic directions for tectonic reconstructions.

5. Discussion

5.1. Magnetostratigraphic correlation and age estimation for the Xingjiawan Fauna

A Late Miocene age for the Xingjiawan Fauna (Zhang, 1993) in the lower part of the section provides a starting point for our integrated bio-magnetostratigraphic correlation. Compared with the number and duration of Late Miocene polarity chrons, the magnetostratigraphic polarity sequence determined for the Xingjiawan section has two plausible correlation options to the GPTS (Hilgen et al., 2012). In the first option, the Xingjiawan polarity sequence is correlated to subchrons C5r.2n to C4n.1n (right-hand side of Fig. 8). The uppermost three normal polarity intervals (N1 to N3) are separated by two reversed polarity intervals (R1 and R2) and provide a reasonable correlation with C4n.1n to C4r.1n of the GPTS. The thick polarity zone N2 is correlated with normal polarity chron C4n.2n, which implies a relatively higher sedimentation rate for this interval. However, this is consistent with the presence of thick conglomerate layers in the lower part of zone N2, which would have been deposited rapidly under high-energy conditions. Beneath, three reversed polarity intervals (R3 to R5) are separated by two normal polarity intervals (N4 and N5), which span from C4r.2r to C4Ar.1r. Further below, the upper boundary of normal polarity zone N6 is the most difficult to correlate with the GPTS. If correlated to the top of chron C5n.2n, four polarity zones (two reversed and two normal) would be missing. Alternatively, when zone N6 is correlated with polarity chrons from C5n.2n to C4Ar.2n, only two short reversed polarity zones are missing. This latter option is deemed more plausible than the former because polarity zone N6 is more likely to contain sedimentary hiatuses than zone R5. A thick conglomerate layer with an erosive base (at a depth of 157–159 m) occurs in the upper part of zone N6, which suggests the presence of a sedimentary hiatus. Furthermore, it is reasonable to correlate zone R5 to a fairly long reversed polarity chron such as C4Ar.1r. Further downward in the section, below the distinctly thick normal polarity interval N6, three pairs of reversed and normal intervals in the lowermost Xingjiawan section correlate well to subchrons C5r.1r to C5r.2n.

In a second correlation option, the Xingjiawan section spans from chron C4An to subchron C3n.3n of the GPTS (left-hand side of Fig. 8). Similar to the first correlation option, the most difficult aspect of the correlation is the thick magnetozone N6. Its best fit to the GPTS is provided by chrons C3Bn–C4n.2n, but now with four reversed polarity zones missing, which would be possible due to minor sedimentary hiatuses (Charreau et al., 2005). Moreover, with this interpretation, the short-duration magnetozones N3 and N7 would have no correlative normal polarity chrons in the GPTS. In addition, correlating magnetozone N2 to subchron C3n.4n suggests a relatively higher sedimentation rate for this interval. In essence, this second correlation option is also consistent with the broad GPTS structure except for the problematic aspects mentioned.

In terms of the number and duration of Late Miocene polarity chrons in the GPTS (Hilgen et al., 2012), the first correlation option is preferable to the second (Fig. 8). Without additional age constraints, however, the possibility of the second option cannot be excluded because several conglomerate layers in the section could be linked to hiatuses and related missing polarity chrons. In both correlation options, the relationship between stratigraphic depth and magnetostratigraphic age is roughly linear, without abrupt shifts (Fig. 9). The linear relationship between depth and age is more evident when the conglomerate layers that represent rapid deposition under high-energy conditions are excluded (Fig. S3). The first and second correlations constrain the sedimentary section to span from ca. 11.6 to 7.6 Ma and from ca. 8.9 to 4.8 Ma, respectively (Fig. 8). However, they correspond to an almost identical

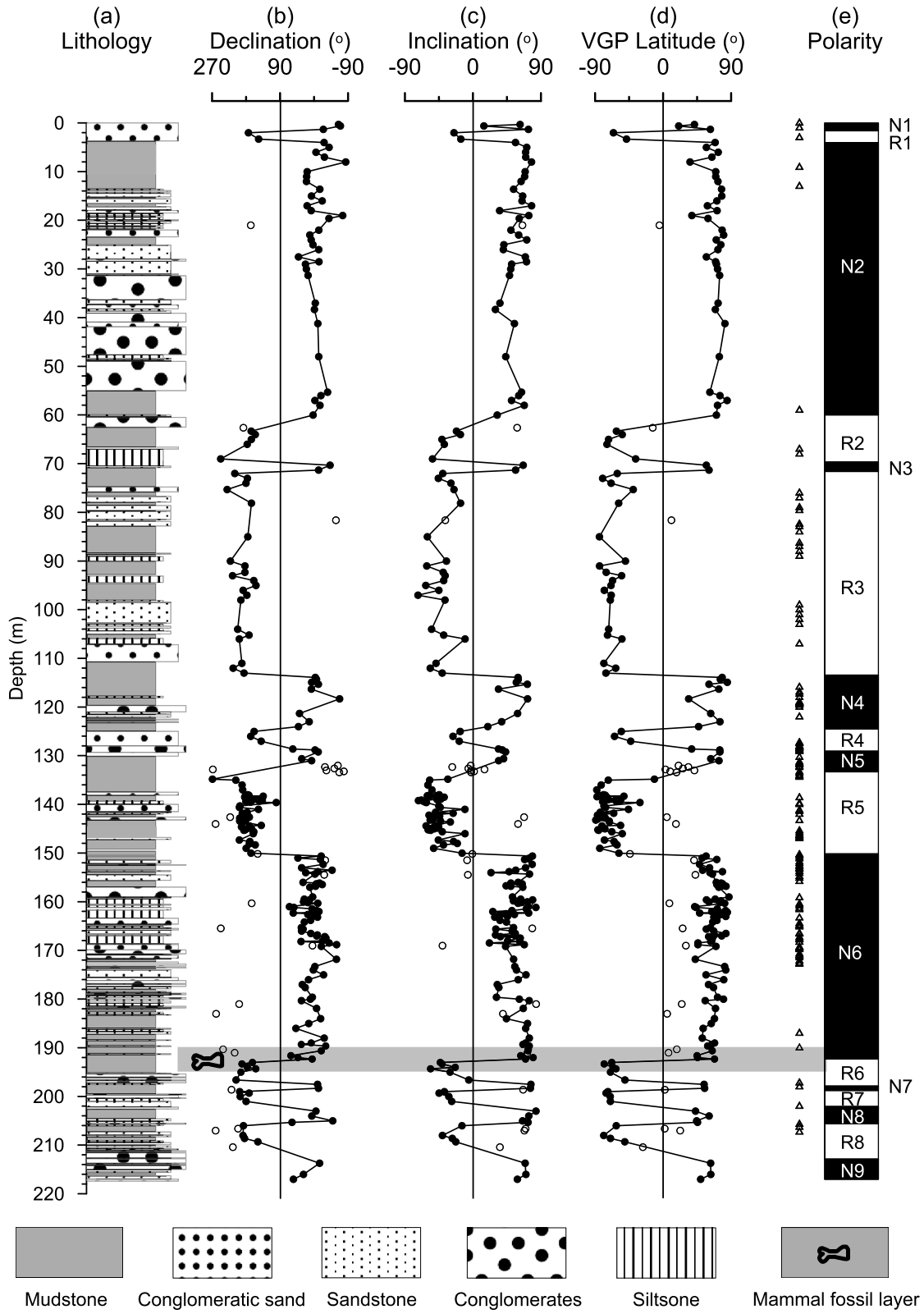

Fig. 5. Lithostratigraphy and magnetostratigraphy of the Xingjiawan section. (a) Lithology, (b) paleomagnetic declination and (c) inclination of the ChRM, (d) VGP latitude, and (e) paleomagnetic polarity sequence of the Xingjiawan section (black = normal polarity; white = reversed polarity). Solid circles represent the reliable paleomagnetic data that are used to establish the Xingjiawan magnetostratigraphy. Open circles represent rejected paleomagnetic data with inclinations $<5°$ or paleomagnetic directions that are inconsistent with the expected geomagnetic field. Open triangles on the left-hand side of the polarity sequence represent rejected paleomagnetic data with unstable demagnetization trajectories at higher temperatures.

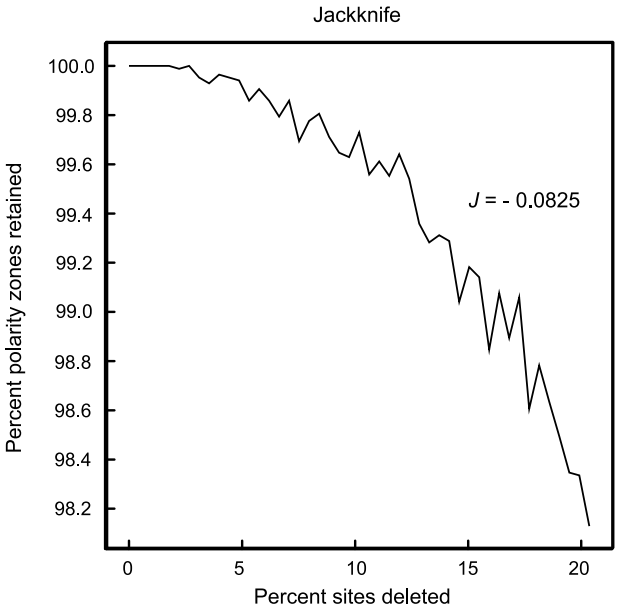

Fig. 6. Magnetostratigraphic jackknife analysis (Tauxe and Gallet, 1991) for the Xingjiawan section. The plot indicates the relationship between average percent of polarity zones retained and the percentage of sampling sites deleted, where the slope (jackknife parameter, J) is directly related to the robustness of a magnetic polarity zonation. The obtained J value of −0.0825 predicts that the Xingjiawan section has recovered more than 95% of the true number of polarity intervals.

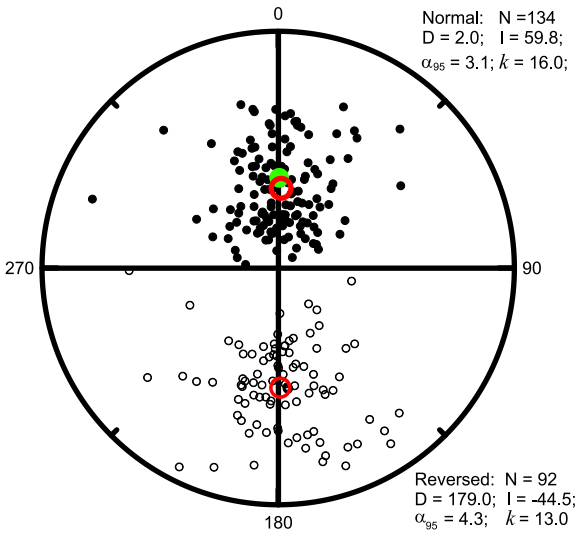

Fig. 7. Equal-area stereographic projection with the 226 accepted ChRM directions after tilt correction. The small solid/open circles represent downward/upward inclinations. The red open circles in the upper and lower planes represent the means of the normal and reversed polarity ChRM directions, respectively. The green solid circle indicates the direction of the present-day geomagnetic field. N = number of samples; D = declination; I = inclination; α_{95} = radius of the 95% cone of confidence about the mean direction; and k = precision parameter. (For interpretation of the references to color in this figure legend, the reader is referred to the web version of this article.)

average sedimentation rate of 53–55 m/Myr, which is comparable to that of the Wangjiashan section (~66 m/Myr) in the Linxia Basin (~50 km south of Lanzhou Basin; Fig. 1) during the Late Miocene (Fang et al., 2003). The lower (113.4–212.8 m) part of the Xingjiawan section has a lower sedimentation rate than the upper (0–113.4 m) part for both options, which is consistent with the coarser-grained nature of the lithologies in the upper section (Fig. 9). Therefore, both correlation options are plausible for the Xingjiawan section, although they each have ambiguities. Late Miocene fluvio-lacustrine sediments in western China seem prone to producing minor magnetostratigraphic ambiguities due to syn-depositional tectonism linked to Tibetan Plateau growth, which generally complicates magnetostratigraphic correlations (Fang et al., 2003, 2005; Sun et al., 2004; Charreau et al., 2005, 2006).

The Xingjiawan Fauna is positioned near the bottom of normal polarity zone N6 and has an unambiguous position in each of the two proposed correlations. In the first option, it is positioned at the boundary between reversed polarity chron C5r.1r and normal polarity chron C5n.2n, with an estimated age of 11–11.1 Ma (Fig. 8). It, thus, correlates to the earliest zone NMU8 (within the Baodean stage) of the Asian Land Mammal Ages (ALMA), to early zone MN9 (within the Vallesian stage) of the European Land Mammal Ages (ELMA) and to zone Cl2 of the North American Land Mammal Ages (NALMA) (Hilgen et al., 2012) (Fig. 8). The second correlation places the mammal fossil layer at around the boundary between reversed polarity chron C4r.1r and normal polarity chron C4n.2n, which yields an age of ~8.1 Ma. It then correlates to middle zone NMU8 (within the Baodean stage) of the ALMA, middle zone MN9 (within the Turolian stage) of the ELMA and zone Hh1 of the NALMA (Hilgen et al., 2012) (Fig. 8). When numerical age constraints were not available in the study of Zhang (1993), the Xingjiawan Fauna was correlated to the younger Turolian stage of the ELMA. Until now, the ALMA is distinctly poorer than the ELMA and NALMA in terms of resolution (Hilgen et al., 2012; Wang et al., 2013). Like the present Xingjiawan Fauna, most Asian faunas are only poorly constrained by their biochronology, and lack more precise numerical ages based on integrated magneto-biostratigraphy. This hampers precise correlation of the ALMA with the ELMA and NALMA, and comprehensive understanding of mammalian evolution worldwide. Precise numerical ages of more Asian faunas are crucial to establish a complete, precise and internationally recognizable Cenozoic ALMA for international land mammal stratigraphy in the future.

5.2. Implications for Stegodon evolution

Stegodon is an elephant-like proboscidean that was fairly common across Asia during the Plio-Pleistocene (Saegusa et al., 2005). The last representatives of the *Stegodon* disappeared in Indonesia (southeastern Asia) at the end of the Pleistocene, about 12,000 yr ago (Van den Bergh et al., 2008). The traditional view is that *Stegodon* originated in Asia during the latest Miocene; a competing hypothesis is that this genus dispersed into Asia from Africa (Shoshani and Tassy, 1996; Saegusa et al., 2005). The latter hypothesis is supported by a fossil *Stegodon* from Kenya, which is dated at 6.7–7.2 Ma with $^{40}Ar/^{39}Ar$ analyses of *in situ* tuffs (Sanders, 1999). It currently represents the oldest known *Stegodon* record. If the traditional view is correct, then there should be *Stegodon* finds in Asia older than that in Kenya. Until now, however, the oldest evidence of *Stegodon* in Asia is from the upper Mahui Formation, Yushe Basin, northwest China (east of Lanzhou Basin; Fig. 1). The find is located in the youngest part of normal polarity chron C3A, with an estimated age of ~6 Ma (Flynn et al., 1997), which is younger than the Kenyan *Stegodon*. The *Stegodon* record from the upper Xianshuihe Formation in Lanzhou Basin is now dated to at least 8 Ma or as early as ~11 Ma (depending on the correlation options discussed), which represents the oldest *Stegodon* find within and outside of Asia. It provides new evidence for an Asian origin (specifically from northwest China) for *Stegodon*. If it did originate from the northeastern margin of the Tibetan Plateau (e.g., Lanzhou Basin), it could have then dispersed to the Yushe Basin and to Africa in the latest Miocene. This finding sheds new light on the origin of *Stegodon*.

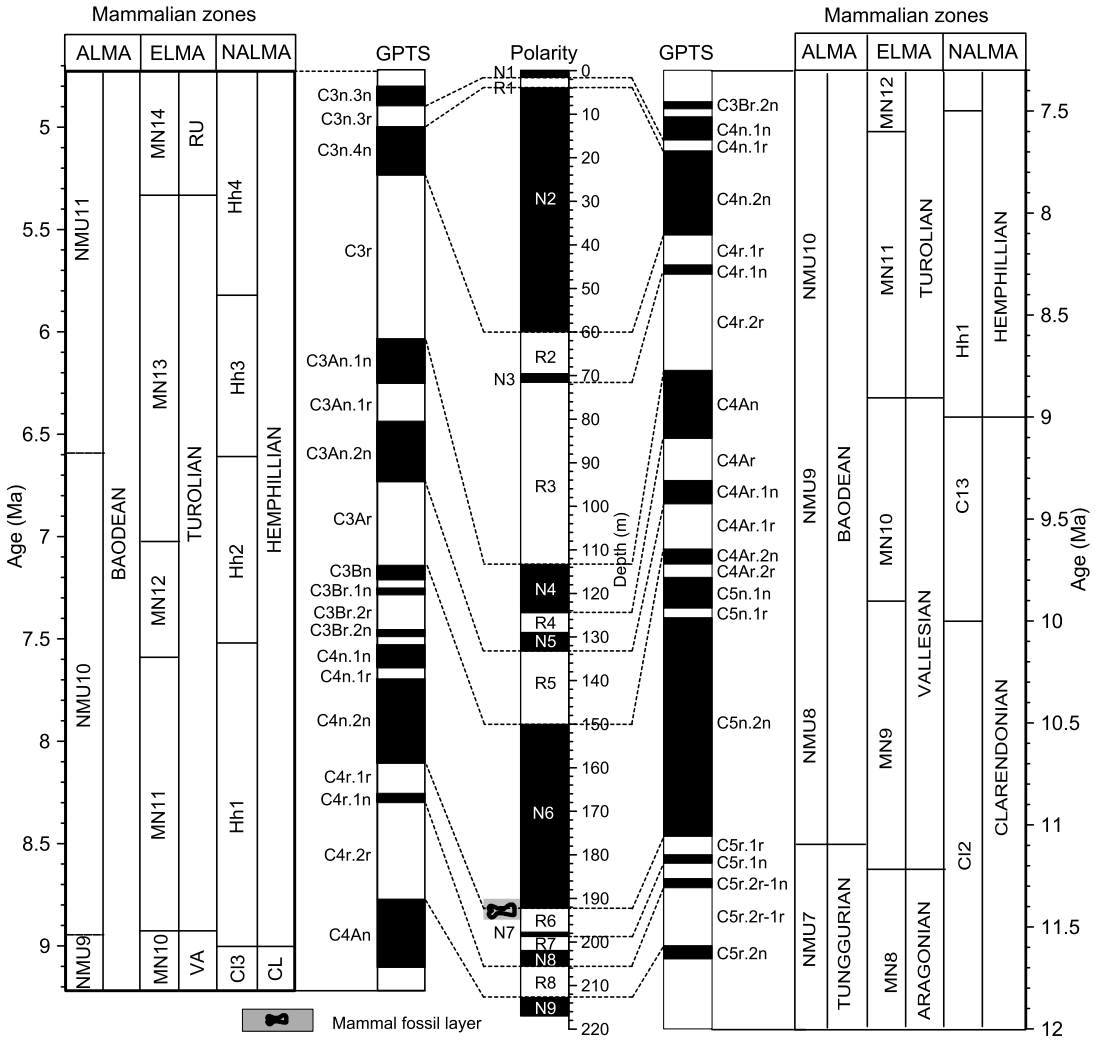

Fig. 8. The two most plausible options proposed for correlation of the observed polarity zones of the Xingjiawan section with the geomagnetic polarity timescale (GPTS) (Hilgen et al., 2012) and with the land mammalian zones of Asia (ALMA), Europe (ELMA) and North America (NALMA) (Hilgen et al., 2012; Qiu et al., 2013). Cl, Clarendonian; Hh, Hemphillian. For paleomagnetic polarity, black = normal polarity and white = reversed polarity.

5.3. Environmental significance of the Xingjiawan Fauna

Until now, Late Miocene paleoenvironments in Lanzhou Basin have largely been unconstrained. Mammals are sensitive to environmental changes, so constraints on the general environmental setting of the Late Miocene Lanzhou Basin can be established by investigating these mammal fossils. Three of the six taxa in the Xingjiawan Fauna (i.e., *Hyaena variabilis*, *Chilotherium haberei* and *Hipparion* sp.) are taxonomically affiliated with typical grazing species that are indicative of an open grassland environment. The other three taxa (*Stegodon* sp., *Chleuastochoerus stehlini* and *Cervidae* indet.) are more adapted to woodland habitats. Therefore, the Xingjiawan Fauna indicates a mixed woodland and grassland setting in Lanzhou Basin during the Late Miocene. Fossil elephants (e.g., *Stegodon*) and rhinoceroses (e.g., *Chilotherium haberei*) contrast with the sparse vegetation and absence of these animals and forests in the modern Lanzhou Basin. This contrast, together with widespread fluvio-lacustrine sediments, implies that Lanzhou Basin was probably warmer and more humid with much denser vegetation during the Late Miocene than today, in order to support large mammals such as rhinoceroses and elephants and other browsing mammals. Such a mixed grassland and woodland setting is also suggested to have occurred in the Late Miocene Qaidam Basin (west of Lanzhou Basin; Fig. 1), as indicated by pollen (Miao et al., 2011) and stable carbon and oxygen isotope records from fossil mammals (Zhang et al., 2012). Pollen records also suggest that the Jiuxi (northeastern margin of the Tibetan Plateau) and Longdong basins (central Chinese Loess Plateau; Fig. 1) had mixed steppe-forest settings with warm and semi-moist Late-Miocene climates (Ma et al., 2005a, 2005b). In addition, in contrast to the Quaternary, the northern hemisphere did not sustain large ice sheets during the Late Miocene (Zachos et al., 2001). Without the influence of northern hemisphere ice sheets, the low-pressure cell over mid-latitude Asia would have been weaker and shifted to the north during the Late Miocene (deMenocal and Rind, 1993; Ao et al., 2012). This would have given rise to an increased intensity and northward expansion of the Asian summer monsoon because of an enhanced temperature gradient between the low pressures over mid-latitude Asia and high pressures over the western Pacific and Australia, with increased moisture transportation from the tropical oceans to northwest China (Ao et al., 2012). Therefore, Lanzhou Basin was unlikely to be as arid as it is today, and precipitation and vegetation were probably substantially more abundant during the Late Miocene.

6. Conclusions

New magnetostratigraphic results suggest that the well-exposed fluvio-lacustrine succession bearing the Xingjiawan Fauna (includ-

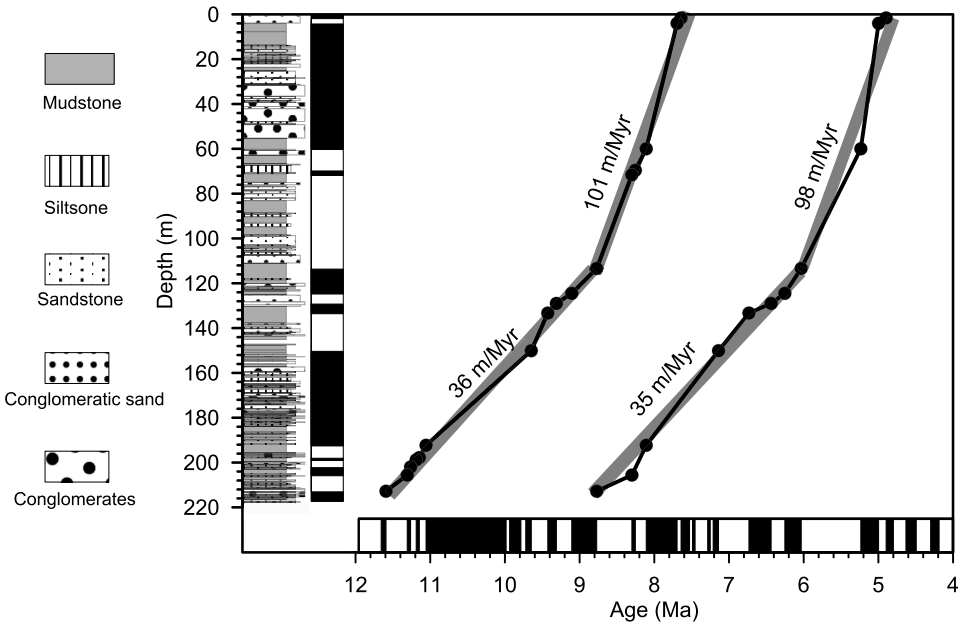

Fig. 9. The relationship between stratigraphic depth and magnetostratigraphic age for the two proposed magnetostratigraphic correlations for the Xingjiawan section. The GPTS of Hilgen et al. (2012) is shown along the age axis (black = normal polarity; white = reversed polarity). Average sediment accumulation rates are similar for the whole section in both options. The lower (113.4–212.8 m) part has a lower sedimentation rate than the upper (0–113.4 m) part in both options, which is consistent with the presence of coarser-grained lithologies in the upper section.

ing a fossil *Stegodon*) in the Lanzhou Basin spans either from ca. 11.6 to 7.6 Ma or from ca. 8.9 to 4.8 Ma. The Xingjiawan Fauna is dated to at least 8 Ma or as early as ~11 Ma, which means that the fossil *Stegodon* in the Lanzhou Basin predates the formerly oldest *Stegodon* find from Africa by at least one million years and perhaps by as many as four million years. This find is the oldest known record of *Stegodon* worldwide, which provides new evidence for an Asian origin of *Stegodon*. Faunal components imply that during the Late Miocene a mixed woodland/grassland setting existed in Lanzhou Basin, in contrast to its modern arid environment.

Acknowledgements

We are grateful to the anonymous reviewers for their insightful comments that helped to improve this paper. This study was financially supported by the National Basic Research Program of China (2013CB956402) and the National Natural Science Foundation of China (41174057, 41290253).

Appendix A. Supplementary material

Supplementary material related to this article can be found online at http://dx.doi.org/10.1016/j.epsl.2015.11.019.

References

Ao, H., Dekkers, M.J., Xiao, G.Q., Yang, X.Q., Qin, L., Liu, X.D., Qiang, X.K., Chang, H., Zhao, H., 2012. Different orbital rhythms in the Asian summer monsoon records from North and South China during the Pleistocene. Glob. Planet. Change 80–81, 51–60.

Charreau, J., Chen, Y., Gilder, S., Dominguez, S., Avouac, J.P., Sen, S., Sun, D.J., Li, Y.G., Wang, W.M., 2005. Magnetostratigraphy and rock magnetism of the Neogene Kuitun He section (northwest China): implications for Late Cenozoic uplift of the Tianshan mountains. Earth Planet. Sci. Lett. 230, 177–192.

Charreau, J., Gilder, S., Chen, Y., Dominguez, S., Avouac, J.P., Sen, S., Jolivet, M., Li, Y.G., Wang, W.M., 2006. Magnetostratigraphy of the Yaha section, Tarim Basin (China): 11 Ma acceleration in erosion and uplift of the Tian Shan mountains. Geology 34, 181–184.

deMenocal, P.B., Rind, D., 1993. Sensitivity of Asian and African climate to variations in seasonal insolation, glacial ice cover, sea surface temperature, and Asian orography. J. Geophys. Res. 98, 7265–7287.

Dunlop, D.J., Özdemir, Ö., 1997. Rock Magnetism: Fundamentals and Frontiers. Cambridge University Press, Cambridge.

Dupont-Nivet, G., Krijgsman, W., Langereis, C.G., Abels, H.A., Dai, S., Fang, X.M., 2007. Tibetan plateau aridification linked to global cooling at the Eocene–Oligocene transition. Nature 445, 635–638.

Fang, X.M., Garzione, C., Van der Voo, R., Li, J.J., Fan, M.J., 2003. Flexural subsidence by 29 Ma on the NE edge of Tibet from the magnetostratigraphy of Linxia Basin, China. Earth Planet. Sci. Lett. 210, 545–560.

Fang, X.M., Yan, M.D., Van der Voo, R., Rea, D.K., Song, C.H., Pares, J.M., Gao, J.P., Nie, J.S., Dai, S., 2005. Late Cenozoic deformation and uplift of the NE Tibetan plateau: evidence from high-resolution magnetostratigraphy of the Guide Basin, Qinghai Province, China. Geol. Soc. Am. Bull. 117, 1208–1225.

Flynn, L.J., Wu, W., Downs, W.R., 1997. Dating vertebrate microfaunas in the late Neogene record of Northern China. Palaeogeogr. Palaeoclimatol. Palaeoecol. 133, 227–242.

Flynn, L.J., Downs, W., Opdyke, N., Huang, K.N., Lindsay, E., Ye, J., Xie, G.P., Wang, X.M., 1999. Recent advances in the small mammal biostratigraphy and magnetostratigraphy of Lanzhou Basin. Chin. Sci. Bull. 44, 105–118.

Hilgen, F., Lourens, L., Van Dam, J., 2012. The Neogene period. In: Gradstein, F.M., Ogg, J.G., Schmitz, M.D., Ogg, G.M. (Eds.), The Geologic Time Scale. Elsevier, Amsterdam, pp. 923–978.

Huang, C.C., 1986. On the palaeoclimate of late Upper Pleistocene in Lanzhou area by analysis of spora and pollen. J. Northwest Univ. 16, 76–83 (in Chinese).

Jiang, H.C., Mao, X., Xu, H.Y., Thompson, J., Wang, P., Ma, X.L., 2011. Last glacial pollen record from Lanzhou (Northwestern China) and possible forcing mechanisms for the MIS 3 climate change in Middle to East Asia. Quat. Sci. Rev. 30, 769–781.

Jiang, Z.X., Liu, Q.S., Zhao, X.Y., Jin, C.S., Liu, C.C., Li, S.H., 2015. Thermal magnetic behaviour of Al-substituted haematite mixed with clay minerals and its geological significance. Geophys. J. Int. 200, 130–143.

Jones, C.H., 2002. User-driven integrated software lives: "Paleomag" paleomagnetics analysis on the Macintosh. Comput. Geosci. 28, 1145–1151.

Kirschvink, J.L., 1980. The least-squares line and plane and the analysis of palaeomagnetic data. Geophys. J. R. Astron. Soc. 62, 699–718.

Kruiver, P.P., Dekkers, M.J., Heslop, D., 2001. Quantification of magnetic coercivity components by the analysis of acquisition curves of isothermal remanent magnetisation. Earth Planet. Sci. Lett. 189, 269–276.

Ma, Y.Z., Fang, X.M., Li, J.J., Wu, F.L., Zhang, J., 2005a. The vegetation and climate change during Neogene and Early Quaternary in Jiuxi Basin, China. Sci. China 48, 676–688.

Ma, Y.Z., Wu, F.L., Fang, X.M., Li, J.J., An, Z.S., Wang, W., 2005b. Pollen record from red clay sequence in the central Loess Plateau between 8.10 and 2.60 Ma. Chin. Sci. Bull. 50, 2234–2243.

Miao, Y.F., Fang, X.M., Herrmann, M., Wu, F.L., Zhang, Y.Z., Liu, D.L., 2011. Miocene pollen record of KC-1 core in the Qaidam Basin, NE Tibetan Plateau and implications for evolution of the East Asian monsoon. Palaeogeogr. Palaeoclimatol. Palaeoecol. 299, 30–38.

Opdyke, N.D., Flynn, L.J., Lindsay, E.H., Qiu, Z.X., 1998. The magnetic stratigraphy of the Yehucheng and Xianshuihe Formations of Oligocene–Miocene age near Lanzhou city, China. In: Proceedings, Paleontology Working Meeting. Lanzhou, p. 51.

Qiu, Z.X., Wang, B.Y., Qiu, Z.D., Heller, F., Yue, L.P., Xie, G.P., Wang, X.M., Engesser, B., 2001. Land mammal geochronology and magnetostratigraphy of mid-Tertiary deposits in the Lanzhou Basin, Gansu Province, China. Eclogae Geol. Helv. 94, 373–385.

Qiu, Z.X., Qiu, Z.D., Deng, T., Li, C.K., Zhang, Z.Q., Wang, B.Y., Wang, X.M., 2013. Neogene land mammal stages/ages of China. In: Wang, X.M., Flynn, L.J., Fortelius, M. (Eds.), Fossil Mammals of Asia: Neogene Biostratigraphy and Chronology. Columbia University Press, New York, pp. 29–90.

Saegusa, H., Thasod, Y., Ratanasthien, B., 2005. Notes on Asian stegodontids. Quat. Int. 126–128, 31–48.

Sanders, W.J., 1999. Oldest record of *Stegodon* (mammalia: proboscidea). J. Vertebr. Paleontol. 19, 793–797.

Shoshani, J., Tassy, P., 1996. The Proboscidea: Evolution and Palaeoecology of Elephants and Their Relatives. Oxford University Press, Oxford.

Sun, D.H., Zhang, Y.B., Han, F., Zhang, Y., Yi, Z.Y., Li, Z.J., Wang, F., Wu, S., Li, B.F., 2011. Magnetostratigraphy and palaeoenvironmental records for a Late Cenozoic sedimentary sequence from Lanzhou, Northeastern margin of the Tibetan Plateau. Glob. Planet. Change 76, 106–116.

Sun, J.M., Zhu, R.X., Bowler, J., 2004. Timing of the Tianshan Mountains uplift constrained by magnetostratigraphic analysis of molasse deposits. Earth Planet. Sci. Lett. 219, 239–253.

Tauxe, L., 1998. Paleomagnetic Principles and Practice. Kluwer Academic Press, Dordrecht, Netherlands.

Tauxe, L., Gallet, Y., 1991. A jackknife for magnetostratigraphy. Geophys. Res. Lett. 18, 1783–1786.

Van den Bergh, G.D., Awe, R.D., Morwood, M.J., Sutikna, T., Saptomo, J.E.W., 2008. The youngest *stegodon* remains in Southeast Asia from the Late Pleistocene archaeological site Liang Bua, Flores, Indonesia. Quat. Int. 182, 16–48.

Wang, X.M., Flynn, L.J., Fortelius, M., 2013. Fossil Mammals of Asia: Neogene Biostratigraphy and Chronology. Columbia University Press, New York.

Xiao, G.Q., Guo, Z.T., Dupont-Nivet, G., Lu, H.Y., Wu, N.Q., Ge, J.Y., Hao, Q.Z., Peng, S.Z., Li, F.J., Abels, H.A., Zhang, K.X., 2012. Evidence for northeastern Tibetan Plateau uplift between 25 and 20 Ma in the sedimentary archive of the Xining Basin, Northwestern China. Earth Planet. Sci. Lett. 317–318, 185–195.

Xie, G.P., 2004. The Tertiary and local mammalian faunas in Lanzhou Basin, Gansu. J. Stratigr. 28, 67–80 (in Chinese with English abstract).

Yue, L.P., Heller, F., Qiu, Z.X., Zhang, L., Xie, G.P., Qiu, Z.D., Zhang, Y.X., 2001. Magnetostratigraphy and paleo-environmental record of Tertiary deposits of Lanzhou Basin. Chin. Sci. Bull. 46, 770–773.

Zachos, J., Pagani, M., Sloan, L., Thomas, E., Billups, K., 2001. Trends, rhythms, and aberrations in global climate 65 Ma to present. Science 292, 686–693.

Zhai, Y.P., Cai, T.L., 1984. The Tertiary system of Gansu province. Gansu Geol. 21, 1–40 (in Chinese).

Zhang, C.F., Wang, Y., Li, Q., Wang, X.M., Deng, T., Tseng, Z.J., Takeuchi, G.T., Xie, G.P., Xu, Y.F., 2012. Diets and environments of late Cenozoic mammals in the Qaidam Basin, Tibetan Plateau: evidence from stable isotopes. Earth Planet. Sci. Lett. 333–334, 70–82.

Zhang, X., 1993. New discovery of the mammalian fossils in Baode period of later Miocene epoch in Lanzhou Basin. Acta Geol. Gansu 2, 1–5 (in Chinese with English abstract).

Zhang, Y.B., Sun, D.H., Li, Z.J., Wang, F., Wang, X., Li, B.F., Guo, F., Wu, S., 2014. Cenozoic record of aeolian sediment accumulation and aridification from Lanzhou, China, driven by Tibetan Plateau uplift and global climate. Glob. Planet. Change 120, 1–15.

Zijderveld, J.D.A., 1967. AC demagnetization of rocks: analysis of results. In: Collinson, D.W., Creer, K.M., Runcorn, S.K. (Eds.), Methods in Paleomagnetism. Elsevier, New York, pp. 254–286.